BABEȘ-BOLYAI UNIVERSITY CLUJ-NAPOCA

FACULTY OH PHYSICS

PhD Thesis Summary

Vibrational studies with biomedical application

Luisa-Mihaela Andronie

Scientific supervisor: Prof. Dr. Onuc Cozar

Cluj-Napoca

2012

Contents

Keywords: FT-Raman, Raman, SERS, Paracetamol normal, Paracetamol sinus Ag nanoparticles, Colon tissue, Adenomacarcinom

Introduction

The used techniques, Raman and IR spectroscopic, together with derivative techniques (micro-Raman, confocal-Raman, surface enhanced Raman (SERS), resonance Raman (RR), or combined (SERRS), combined with IR absorption spectroscopy, provide valuable information about the structure, properties, dynamics, molecular identity of certain species in different biological media and their willingness to interact with other species or to be absorbed on noble metal nanostructures.

Vibrational spectral techniques offer several advantages in the context of current research, because of special sensitivity, they can be ideal ways to achieve very fast tools, noninvasive and affordable for an early diagnosis of diseases as sample preparation and measurement are very simple, and acquisition time is very short.

The present thesis deals with the original experimental studies on molecular structures used in pharmaceutical formulation (Tylenol-trade) and that of complex biological systems (human colon tissue) using vibrational spectroscopic techniques. We analyzed several molecular species with antipyretic and analgesic effects in various pharmaceutical formulations to test the potential of the techniques in monitoring and detection of these species under physiological conditions.

Biological activity and pharmaceutical properties of drugs highly depend on their structure. After the experiments it was found that paracetamol taken in overdose, can cause hepatic necrosis in both humans and animals used in experiments [1, 2]. Alcohol is favorable for liver damage, damage caused also by big therapeutic doses of paracetamol [3]. Because of toxic side effects, paracetamol was the subject of many toxicological studies [4, 5]. In contrast to aspirin, paracetamol is believed to act almost exclusively on the central nervous system with low peripheral effects.

Starting from the idea that the evolution of the disease is accompanied by changes in terms of chemistry / biochemistry of cells, tissues, organs or fluids of the bodies, vibrational spectroscopy may be the best conventional method for ultra sensitive detection of these changes, which would be detected before morphological and systemic manifestations allow clinical diagnostic by conventional methods. For example, colon cancer, which is the subject of this paper, is found on anatomic imaging techniques such as endoscopy, ultra sensitive technique, followed by histopathological examination of biopsy. These conventional diagnostic methods are often applied in years of early stage disease, which generates an irrecoverable delay in applying an effective treatment. If detected early the disease is one of the most easily curable with a survival rate of 90%, thus detecting it early and subjected to an appropriate treatment scheme it would save many lives

Chapter 2. Raman and SERS studies on paracetamol molecule

2. 1. Characterization physico-chemical and differentiation of species of paracetamol (normal and sinus)

The chemical structure of paracetamol ($C_8H_9NO_2$) is exposed in the Fig. 2.1 this is indicated for the relief of mild-to-moderate pain, and for the reduction of fever and is a major component of many over-the counter analgesics and cold and flu remedies.

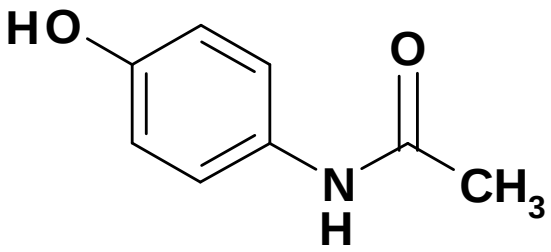

Fig. 2.1. Molecular structure of paracetamol.

Furthermore, it is known that alcohol may predispose to liver damage caused by therepeutic doses of paracetamol [6] Because of these toxic side effects paracetamol has been subject to many toxicological studies [7, 8]. Previous studies shown that long-therm, daily use of paracetamol is associated independentely with an increased risk of renal disease [9] and causes an immediate and highly specific inhibition of replicative DNA synthesis [10].

Paracetamol, can crystallize in three different polymorphic forms known as Form I, II, and III. [11-16] The monoclinic form (form I) is the normal markete form [17, 18] the form II was identified by recristallization from an ethanolic solution and corresponds to an orthorhombic form [19] and the form III was mentioned as a very unstable form], which cannot be studied due to its unstability. The metastable polimorphs of paracetamol are of particular industrial interest because the commercial form requires binders for tablet formation [20, 21]. The form I of paracetamol is stable at ambient temperature and pressure [22, 23] while the orthorhombic form of paracetamol is suitable for direct compression tableting and may also be slightly more soluble but has been crystallized only in small quantities and the only commercially available form is the monoclinic form of paracetamol, the thermodinamically most stable modification [24-26].

Numerous IR [27-31] and Raman [32, 33] studies are already recorded in order to characterize and identify the three metastable forms of paracetamol the transition between them, and the comparison between tablets and solutions [34].

In the present work, based on the vibrational Raman characterization of paracetamol tablets, I tryed to distinguish the various molecular species mode in terms of pH value, the adsorption manner to the silver colloidal nanoparticles, to establish the functional groups involved in adsorption and to check the possibility to monitor low dosage level using SERS spectroscopy.

2. 2. Experimental preparation of solutions and surfaces

Pharmaceutical tablets of paracetamol commercially available (Europharm), as normal and sinus (500 mg), were employed in our study without further purification. The paracetamol solutions were prepared by tablet dissolving in distilled water at room temperature.

The island films, which we used in our measurements as SERS substrates, were prepared through thermal evaporation, and the films that were obtained have different particles roughness (1.9 and 2.9 Å) [35]. For the SERS samples processing we have dropped paracetamol solutions, in that order on the film surfaces, and then we kept drying for a number of minutes. As soon as the drop becomes drying, we can focalise the laser spot on this position.

The FT-Raman spectra were obtained by using a Equinox 55 spectrometer with an integrated Bruker (D) FRA-106/S Raman module and a resolution of 2 cm^{-1}. The 1064 nm radiation from a Nd-YAG laser with an output of 390 mW was employed for the excitation. A Ge detector operating at liquid nitrogen temperature was used. The number of scans was 200.

The Raman and the SERS spectra on island films were recorded with a Dilor Raman microspectrometer (Horiba-Jobin-Yvon, model LabRam) using the 514.5 nm excitation line from an argon ion laser (Spectra Physics, model 2016). The spectra were collected in the backscattering geometry using a microscope equipped with an Olympus LMPlanFL 50x objective with a spectral resolution of 5 cm^{-1}. The detection of Raman signal was carried out with a Peltier-cooled CCD camera and for the signal aquisition was employed the analysing software package LabSpec. The laser power varied from 100 to 200 mW is indicated for each figure caption.

2. 3. The Raman spectra of paracetamol in various pharmaceutical formulations

The commercial normal and sinus paracetamol drugs were investigated with Raman spectroscopies to stand out the presence of monoclinic and orthorhombic forms of paracetamol in the solid state, in aqueous solution, and on the glass surfaces after recrystallization. The vibrational fundamentals from the FT-and micro-Raman spectra, presented in Fig. 2.2, were analyzed by comparing these vibrational modes with those from the literature [36-43].

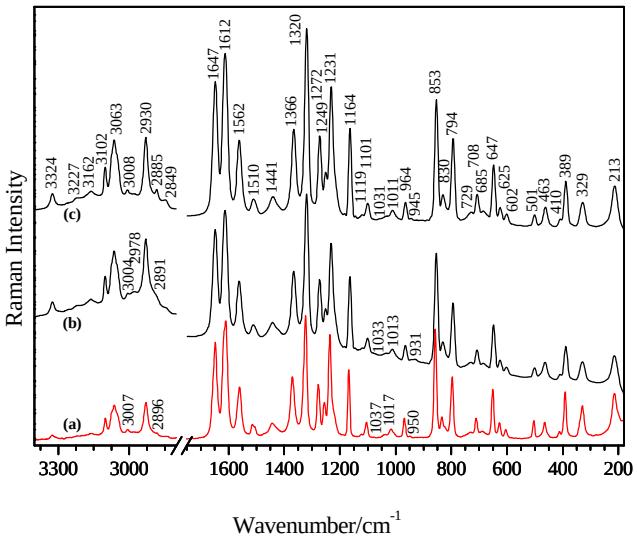

Fig. 2.2. FT-Raman (a) and micro-Raman (b,c) spectra of normal (a,b) and sinus (c) tablets of paracetamol. Excitation: 1064 nm, 390 mW (a); 514.5 nm, 100 mW (b,c).

Furthermore the peaks at 1562 and 1510 cm^{-1} were assigned to the C-N amide stretching modes, while the bands at 1612 and 1441 cm^{-1} were attributed to the C-C aromatic stretching modes. These frequencies together with them assignment are specific for the monoclinic form I of the paracetamol [44]. For this form some particular peaks are present at 1231, 794 and 708 cm^{-1}, peaks which correspond to the phenyl-N stretching mode, to the out-of-plane deformation mode of p-substituted aromatic system and to the out-of-plane CN-H and phenyl deformation modes, respectively [45, 46]. Other characteristic frequencies of the form I of paracetamol, which can be seen in the FT- and micro-Raman spectra of the solid state are the medium band at 1272 cm^{-1}, which was assigned to the C-O stretching mode [47] and the weak medium peak at 463 cm^{-1} that can be attributed to the skeletal bending mode [45]. The form I of paracetamol has Raman bands at 1272, 1231, 708, 463 and 213 cm^{-1}, which are not present in the spectrum of the form II. On the other hand, the spectrum of the form II could have bands at 1185, 454 and 201 cm^{-1}, which are not present in the spectrum of the formI. Taking into account all these characteristic Raman bands, i can figure out the presence of the monoclinic form in both, normal and sinus, paracetamol tablets.

When one tablet of each paracetamol type was dissolved in 10 ml distilled water and after that one drop of the solution was kept drying on the glass, the paracetamol recrystallizes and the Raman spectra of both paracetamol forms look quite different (Fig. 2.3a, b). The weak medium peak detected at 3324 cm^{-1} in the solid state are now rather shifted, at 3325 cm^{-1} for the normal paracetamol and at 3323 cm^{-1} for the paracetamol sinus. This weak difference (1 cm^{-1}) is enough to assert that the band at 3325 cm^{-1} is specific to the orthorhombic form of

the paracetamol. In the same case, the bands at 1559, 1099, 725 and 622 cm^{-1} (Fig. 2.3a) are typical for the orthorhombic form of paracetamol, whereas the peaks at 1562, 1101, 730 and 623 cm^{-1} (Fig. 2.3b) are more specific for the monoclinic form of the paracetamol [46]. Other remaining bands of the spectra are, as previous discussed, attributed to the monoclinic form of the paracetamol. In this case, one can assume that after recrystallization, the normal paracetamol includes a mixture between monoclinic and orthorhombic forms.

Looking at the Raman spectra of normal and sinus paracetamol on the glass surfaces after recrystallization (Fig. 2.3), one can observe the enhancement of some bands in comparison with the Raman spectra of the tablets, where the Raman signal seems to be quite similar for both types of paracetamol. The enhancement of the band at 2883 cm^{-1} (paracetamol sinus, Fig. 2.3b) can be due to the presence of the cellulose, lactose, talc, stearic acid and magnesium stearate, which normally have very strong bands in the 2870 -2895 cm^{-1} spectral range [48-55].

In the same spectrum, the peaks at 708 and 388 cm^{-1} (Fig. 2.3b) increase in 3 relative intensity compared to the spectrum of the normal paracetamol (Fig. 2.3a) and to the spectra of the tablets (Fig. 2.2).

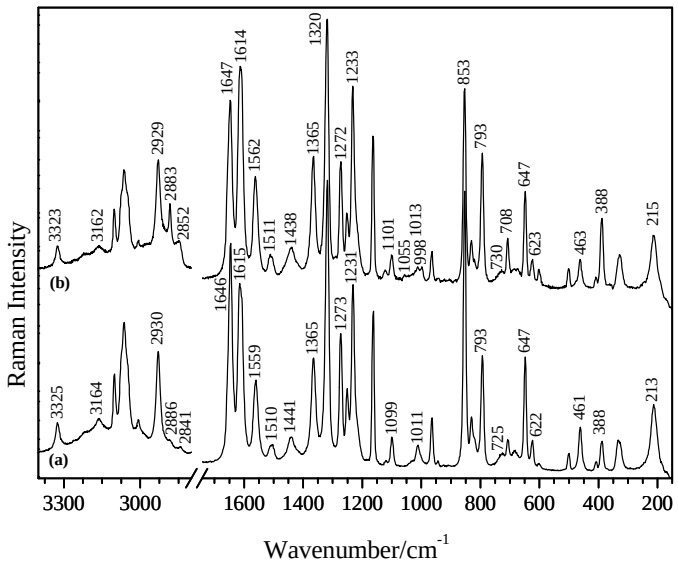

Fig. 2.3. Micro-Raman spectra of recrystallized normal (a) and sinus (b) paracetamol. Excitation: 514.5 nm (a,b), 200 mW (a,b).

These increases can be produced because of the lactose, which has strong peaks in the range of 864-698 cm^{-1} and 357-377 cm^{-1}, because of the cellulose that extends substantial

bands around 382 cm^{-1}, and because of the maize starch, which give a superior band near to 360 cm^{-1} [56-60].

The pH dependence Raman spectra of normal and sinus paracetamol aqueous solutions in the basic and acidic pH range are presented in Figs. 2.5, 6 and 7, 8, respectively. In the Raman spectra of normal paracetamol solution at basic pH values (Fig. 2.5) a significant broadening of the 1619 cm^{-1} band together with its two neighboring shoulders, at 1696 and 1660 cm^{-1}, is observable.

This band, in the basic pH range, is 12 cm^{-1} red shifted (1606 cm^{-1}) and may be assigned to the asymmetrical C=C aromatic and C-N stretching modes (Fig. 2.5, pH13); the shoulders at 1696 and 1660 cm^{-1}, attributed to the CNH and C=O (amide I) stretching modes, are importantly red shifted at higher pH values (1689 and 1637 cm^{-1}, Fig. 2.5, pH13).

The weak band at 1568 cm^{-1}, 20 cm^{-1} red shifted in the basic pH range, can be due to the in-plane N-H bending mode (amide II).

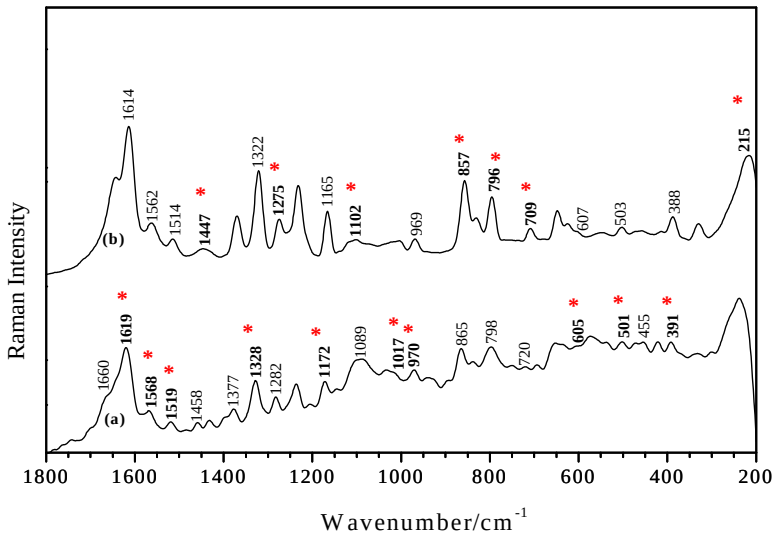

Fig. 2.4. Raman spectra of normal (a) and sinus (b) paracetamol solution ($3.3x10^{-1}$ M). Excitation: 514.5 nm (a,b), 200 mW (a,b).

By analogy with the normal paracetamol, in the Raman spectra of the sinus paracetamol at basic pH values (Fig. 2.6) a significant increasing in relative intensity and 14 cm^{-1} red shift of the band at 1614 cm^{-1}, which is attributed to the C=C aromatic and C-N stretching modes, can be observed (Fig. 2.6, pH13).

Moreover, the strong band at 1643 cm^{-1} that corresponds to the C=O (amide I) stretching mode, decreases in relative intensity, becomes a shoulder beginning with pH 10.5

and is 15 cm^{-1} red shifted; the weak medium band at 1562 cm^{-1} becomes broader, is 22 cm^{-1} red shifted, and can be due to the in-plane N-H bending mode (amide II) (Fig. 2.6, pH13).

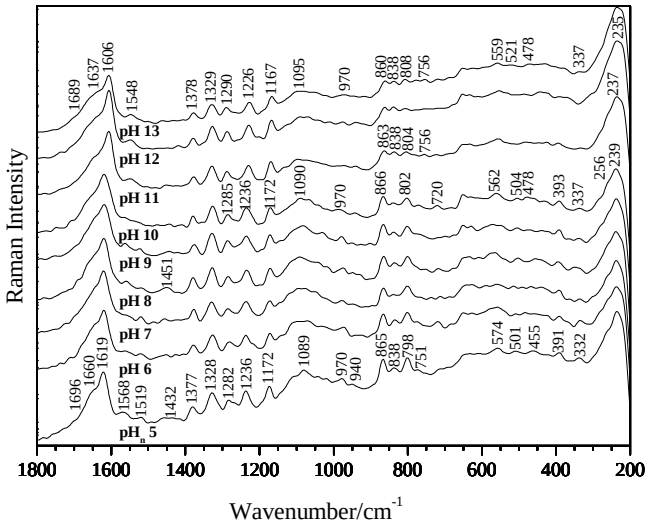

Fig. 2.5. Raman spectra of $3.3x10^{-1}$ M normal paracetamol solution at different basic pH values. Excitation: 514.5 nm, 200 mW.

Furthermore, the weak signal at 1432 cm^{-1}, as a contribution of the asymmetrical CH_3 bending and phenyl stretching modes of the normal paracetamol, becomes broader and is 29 cm^{-1} blue shifted in the basic pH range. The medium band at 1377 cm^{-1} is slightly decreased in relative intensity and is attributed to the symmetrical CH_3 bending mode. The signal correspondent to the C-N stretching mode (amide III) (1328 cm^{-1}) decreases in relative intensity, whereas the band correspondent to the C-O and C-N stretching modes (1282 cm^{-1}) increases in relative intensity in the basic pH range (Fig. 2.5, pH13). With the pH increase, one can observe, first a broadening and then a red shifting (20 cm^{-1}) of the phenyl-N bending mode (1236 cm^{-1}), in comparison to the adjacent band at 1172 cm^{-1}, assigned to the phenyl-N and COH bending modes, which remain almost constant in relative intensity in the basic pH range (Fig. 2.5) and is slightly red shifted (5 cm^{-1}).

In contrast to the normal paracetamol, in the Raman spectra of the sinus paracetamol (Fig. 2.6), the weak peak at 1447 cm^{-1}, with the same assignment as for the normal paracetamol, seems to increase in relative intensity at pH 8 and after that, beginning with pH 9 becomes broader and disappear at higher pH values. The next two bands (1369 and 1323 cm^{-1}) in the Raman spectra of the sinus paracetamol, which were attributed as for the normal paracetamol, decrease in relative intensities and are slightly blue shifted.

The following peak at 1275 cm^{-1} is 5 cm^{-1} blue shifted and increases in relative intensity, whereas the signal at 1233 cm^{-1} becomes broader, is slightly decreased in relative

intensity and 10 cm^{-1} red shifted (Fig. 2.6, pH13). The bands at 865, 838 and 798 cm^{-1} from the Raman spectra of normal paracetamol (Fig. 2.5, pH 5 to 10) are slightly decreased in relative intensity, become weaker with the pH increasing, and are slightly shifted; they are attributed to the out-of-plane C-C skeletal deformation, to the out-of-plane C-H bending mode and to the phenyl-N bending mode, respectively. Similar bands from the Raman spectra of the sinus paracetamol observed at 857, 831 and 796 cm^{-1} (Fig. 2.6), decrease in relative intensity, are changed in shape and are slightly blue shifted. The weak band at 574 cm^{-1}, which corresponds to the out-of-plane phenyl-N deformation mode of the normal paracetamol, is slightly decreased in relative intensity and 15 cm^{-1} red shifted in the basic pH range (Fig.2.7, pH13), whereas in the case of sinus paracetamol, the analogous band at 547 cm^{-1} decreases in relative intensity and then disappears (Fig. 2.6, pH 9-13). In general, all bands due to the C-N, N-H, phenyl-N, COH and C=O vibrational modes of paracetamol, become weaker and are red shifted.

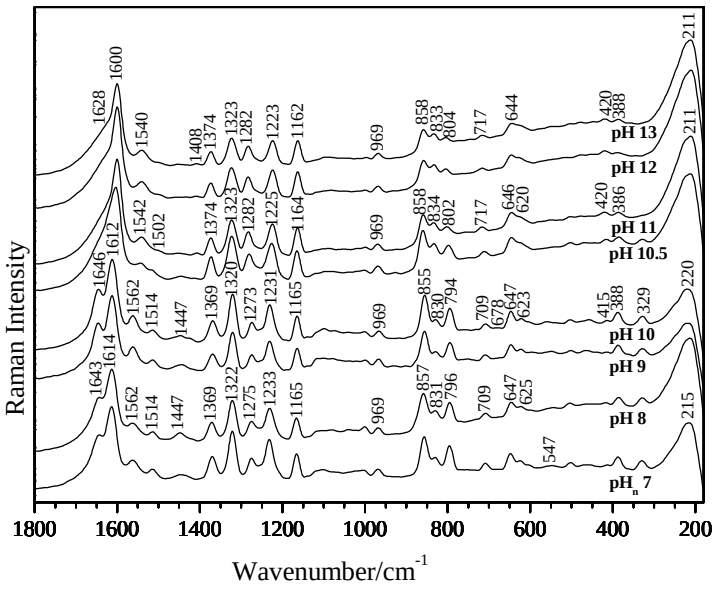

Fig. 2.6. Raman spectra of $3.3x10^{-1}$ M sinus paracetamol solution at different basic pH values. Excitation: 514.5 nm, 200 mW.

Can perceive that the out-of-plane phenyl-N deformation mode (574 cm^{-1}) is represented by two weak peaks at pH 3 (572 and 549 cm^{-1}) (Fig. 2.7) and at pH0 remains a unique band, which is 17 cm^{-1} red shifted (557 cm^{-1}). Thus, the fully protonated normal paracetamol molecule predominates at low pH values [62]. Finally, taking into account the major changes in the band shape attributed to phenyl-N Raman bands at acidic pH values, a protonation of the NH group is very likely [63].

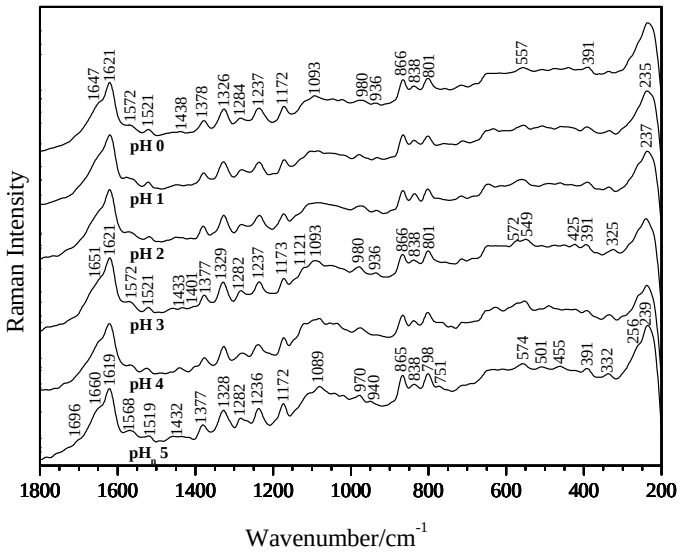

Fig. 2.7. Raman spectra of $3.3x10^{-1}$ M normal paracetamol solution at different acidic pH values. Excitation: 514.5 nm, 200 mW.

Comparing Figs. 2.6 and 2.8, the Raman spectra of the sinus paracetamol remain unchanged in the pH range from 7 to 0, which demonstrate that at the neutral pH7, the sinus paracetamol exists in the zwitterionic form.

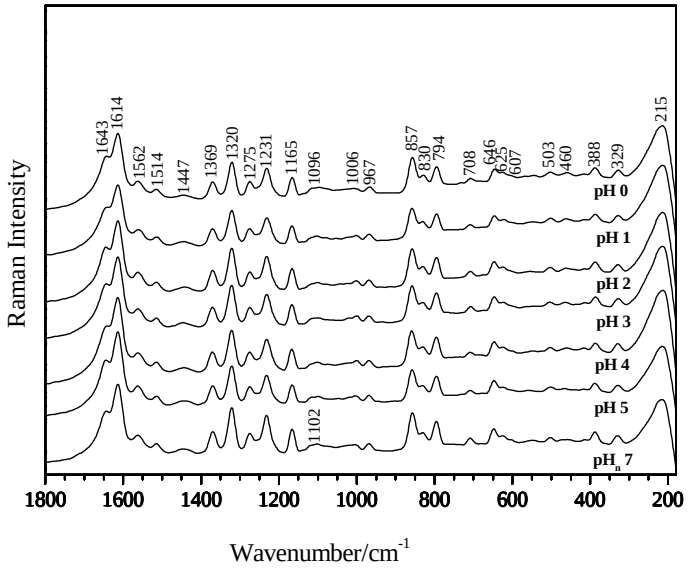

Fig. 2.8. Raman spectra of $3.3x10^{-1}$M sinus paracetamol solution at different acidic pH values. Excitation: 514.5 nm, 200 mW.

2. 4. SERS spectra of the paracetamol on silver island films

The SERS spectra of normal and sinus paracetamol aqueous solutions ($8x10^{-2}$ M) are presented in Figs. 2.9 and 2.10 in comparison with the Raman spectra of the bulk solutions

($3.3x10^{-1}$ M) at pH5 and pH7, respectively. Large differences in band positions and relative intensities are observed, allowing the assumption of a chemisorbed species.

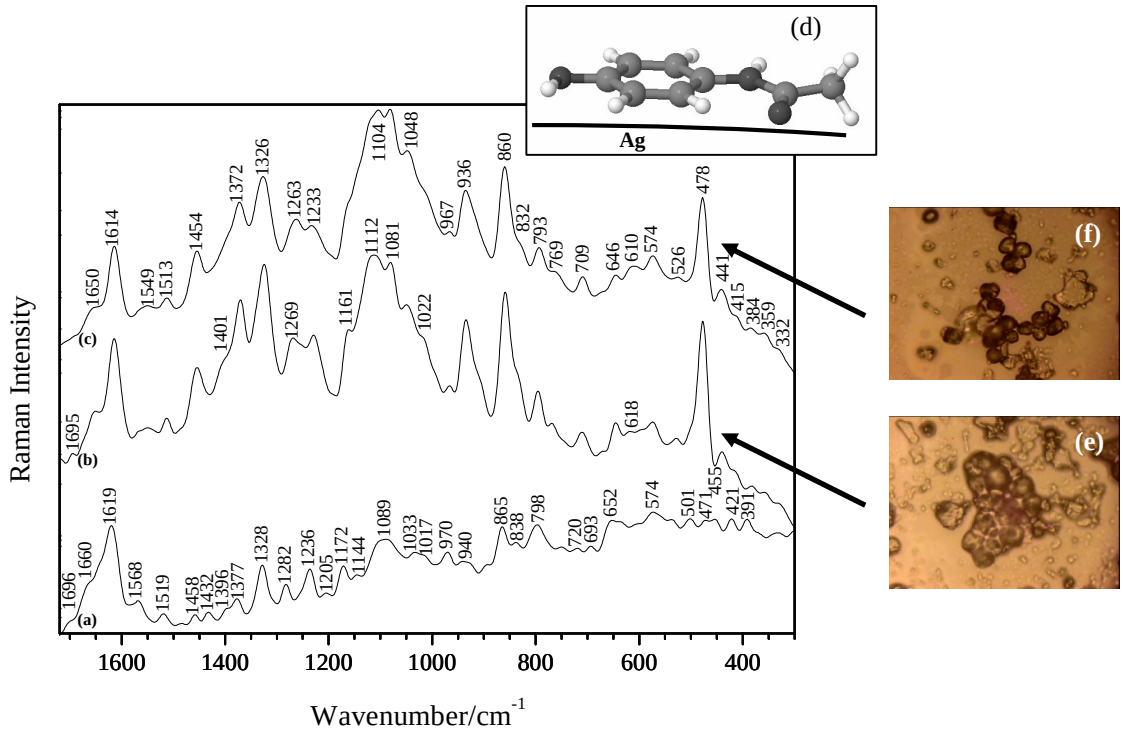

Fig. 2.9. SERS spectra of $8x10^{-2}$ M normal paracetamol on thin silver films of 1.9 Å (a) 2.9 Å (b) roughnesses together with the microscopical images of the measured regions (e), (d) and its proposed orientation on the silver surface (f). Raman spectrum of $3.3x10^{-1}$M normal paracetamol solution (pH 5) (c). Excitation: 514.5 nm (a-c), 200 mW (c) and 50 mW (a,b).

The SERS spectra were recorded on two types of Ag island films with different roughness (2.9 and 1.9 Å) [64]. Microscopic images of paracetamol solutions on both types of thin films can be seen in Fig. 2.9 e, f and Fig. 2.10 e, f. The medium bands observed in the SERS spectra of normal paracetamol at 1263 and 1233 cm^{-1} (19 and 3 cm^{-1} red shifted from the Raman spectrum of the solution) are due to the C-N and phenyl-N stretching modes of the amide group and present changes in the band shape.

In the case of the sinus paracetamol (Fig. 2.10), the medium bands observed in the SERS spectra at 1270 and 1233 cm^{-1} (5 and 2 cm^{-1} red shifted from the Raman spectrum of the solution) have the same assignment as for the normal paracetamol and show changes in the shape as well. The medium bands at 1172 cm^{-1} (for the normal paracetamol) and at 1164 cm^{-1} (for the sinus paracetamol) in the Raman spectrum of the solution, become shoulders in the SERS spectra and are 11 and 1 cm^{-1} red shifted, being attributed to the C-OH bending modes.

The medium signal at 1089 cm^{-1} in the Raman spectrum of the normal paracetamol solution (Fig. 2.9) is split in the SERS spectrum in three peaks and one shoulder (1104, 1081,

1048 and 1022 cm^{-1}), which were assigned to the C-OH stretching, asymmetrical C-O-C stretching, CCC bending, and C-OH and phenyl bending modes, respectively.

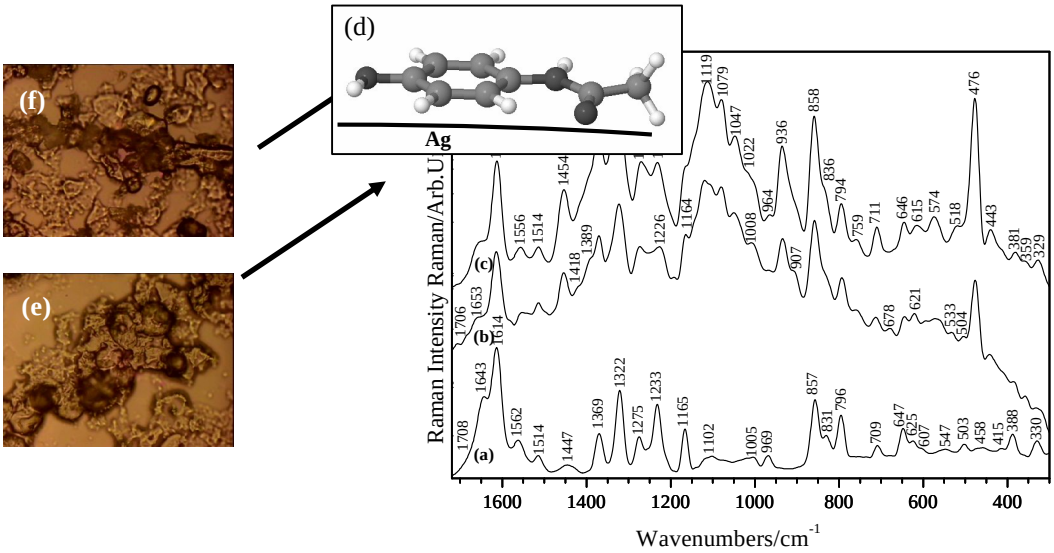

Fig. 2.10. SERS spectra of $8x10^{-2}$ M sinus paracetamol on thin silver films of 1.9 Å (a) 2.9 Å (b) roughnesses, together with the microscopical images of the measured regions (e), (d) and its proposed orientation on the silver surface (f). Raman spectrum of $3.3x10^{-1}$M sinus paracetamol solution (pH 7) (c). Excitation: 514.5 nm (a-c), 200 mW (c) and 50 mW (a,b).

In this case, according to the surface selection rules [66], the amide I, II, and III bands are expected to be enhanced. Another possibility for paracetamol to chemisorb is through the π electrons of the phenyl ring. In accordance to the electromagnetic selection rules proposed by Creighton [65] and Moskovits and Suh [66], the C-H stretching mode should be relatively enhanced when the C-H bond is perpendicular to the metal surface plane, as compared to the case in which the C-H bond lies parallel to the surface.

The nitrogen interaction with the silver surface is shown by the enhancement of the amide group vibrations. More specifically, the very intense bands in the SERS spectra at 1454, 1372 and 1326 cm^{-1} for the normal paracetamol (Figs. 2.9.a,b); 1454, 1371 and 1326 cm^{-1} for the sinus paracetamol (Figs. 2.10.a,b), red and blue shifted, respectively, from the Raman spectra of the bulk solution assigned to the symmetrical C=O stretching mode (amide I), to the H_3C-C=O stretching and symmetrical CH_3 bending modes and to the C-N stretching (amide III) mode, are preponderantly due to the amide group, showing its close vicinity to the Ag surfaces.

A flat orientation of the phenyl ring to the metal surface (Figs. 2.9f, 2.10f) is supported by the intense band due to the Ag-π electrons of phenyl bond, which can be detected at 478 cm^{-1} and 440 cm^{-1} for the normal paracetamol and at 476 cm^{-1} and 443 cm^{-1} for the sinus paracetamol, respectively, considering both silver film roughnesses.

The flat orientation of the phenyl ring is also supported by the importantly increase in relative intensity of the band at 936 cm^{-1} (in the SERS spectra of both normal and sinus paracetamol, Figs. 2.9a,b and 2.10a,b), which is due to the out-of-plane C-H deformation of the phenyl ring, by the highly increase in relative intensity of the bands at 860 cm^{-1} (SERS spectra of normal paracetamol) and 858 cm^{-1} (SERS spectra of sinus paracetamol), which were attributed to the C-H and C-C out-of-plane skeletal deformations.

Taking into account the surface selection rules and the reported literature data, we were able to give a reasonably explication of the adsorbate structures on the Ag metal surfaces from the SERS spectra. A strong chemical interaction of both types of paracetamol (normal and sinus) with the silver island films is realized through the lone pair electrons of the nitrogen atoms from the amide group and the π electrons of the phenyl ring, in a flat orientation

Chapter 3. Raman techniques applied to study complex biological systems (cells, tissues)

3. 1. General on the investigated tissue structure and their evolution in human colon cancer

Adenocarcinoma is a malignant epithelial tumor, originating from glandular epithelium of the colorectal mucosa. Colon cancer is currently the third leading cause of cancer related deaths in the Western world with 655.000 deceased worldwide per year. Study of colon cancer is showing a specific changes in nucleic acid, protein lipid and carbohydrate quantitities and/or conformation, characteristized the neoplastic cells [67].

Current cancer diagnosis is based on various expensive and time-consuming medical imaging techniques such as magnetic resonance imaging, computerized tomography, ultrasonography, which are followed by histopathological examination of a biopsy specimen taken from the patient. More accurate analysis and elucidation of cancer mechanism could be achieved by using spectroscopic techniques which probe the molecular content of the investigated samples.

3. 2. Theoretical and experimental method

Tissue samples were isolated from human ascending colon specimen obtained within 2 h after resection from a patient (only one patient) that underwent surgery. Ethical approval has been obtained in order to study human sample tissues. Standard histopathological examination confirmed adenocarcinoma. Freshly collected carcinoma tissues were preserved in phosphate-buffered formalin solution (10%) about 2 h, up to the spectroscopic

measurements. Samples were fixed in formalin and it was shown that this procedure did not alter the observed Raman peaks of the tissue, and was therefore a suitable method of fixation. Thin cross-sectioned pieces from normal and adenocarcinoma colon tissue were selected for spectral data acquisition. The samples were transversely sectioned to the colon wall, and revealed three distinct zones with brown, yellow, and white aspect respectively, corresponding to the outer to inner colon wall, where the epithelial layer distortion due to carcinogenesis was evident.

Thin freshly sectioned layers were isolated and placed under Raman microscope for the optical microscopy and micro-Raman measurement. Then, microdroplets of colloidal silver nanoparticles obtained using the Lee-Meisel method [68] were added to the tissue surface for SERS acquisition. Laser focus followed the Ag-dropped point.

The micro-Raman and SERS spectra were recorded with a Dilor Raman microspectrometer (Horiba-Jobin-Yvon, model LabRam) using 632.8-nm excitation line from a He-Ne laser. The spectra were collected in backscattering geometry using a microscope equipped with an Olympus LMPlanFL 50x, 10x objective with a spectral resolution of 2 cm^{-1}. The detection of Raman signal was carried out with a Peltiercooled

CCD camera and for the signal acquisition, the analyzing software package LabSpec was employed. The laser power at the sample varied from 15 to 25 mW and 10 cycles of 2 s were accumulated. Microscopic examination using 10x or 50x objectives was performed before and after laser exposure in order to monitor possible morphological changes induced by the laser beam on the focused point. The optical image of the tissue was found unchanged upon laser exposure. A video camera assisted the tissue behavior under laser exposure.

The FT-IR spectra were obtained by using an Equinox 55 Bruker spectrometer with an integrated Raman module (Bruker, FRA106), fiber optic coupled to a Raman scope II module. The spectral data were analyzed using the OPUS 2.0.5 and Origin 6.0 software.

3. 3. Results obtained by investigating colon tissues using FT-IR spectroscopy

Several studies on normal, premalignant (polyp) and malignant human colonic tissues from patients with different stages of malignancy, was reported. This studies used a method which is based on microscopic infrared study (FT-IR-microscopy) of thin tissue specimens and a direct comparison with traditional histopathological analysis, which serves as a “gold” reference [69].

FT-IR spectroscopy has proven to be a potent analytical tool for studying complex biological materials such as tissues, body fluid and cell cultures [70].

In Fig.3.1 are presented the FT-IR spectra acquired from the yellow areas from both normal and cancerous samples, this representing the inner part of the human colon.

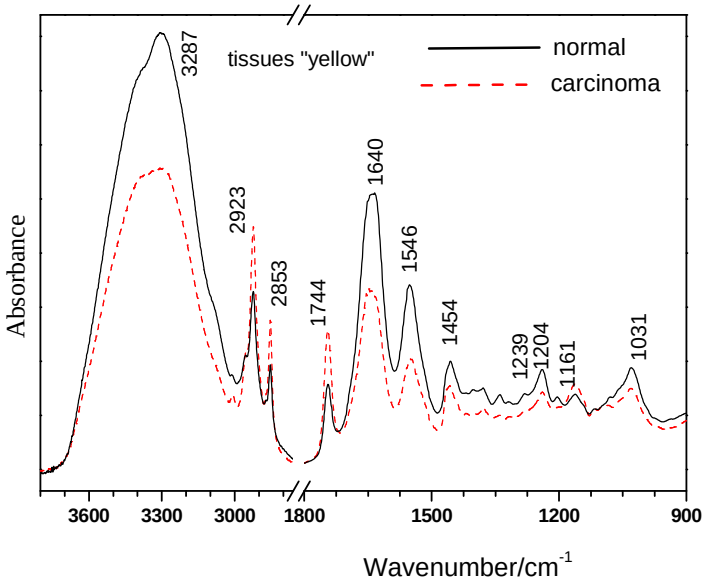

Fig. 3.1. ATR- FT-IR spectra of the normal (upper) and carcinoma colon section (lower) acquired from yellow tissues.

In the big wavenumber spectral range, slight differences in the amide A band assigned to N–H stretching mode of proteins can be seen at 3287 cm^{-1} in the normal tissue. In the small wavenumber range the amide I and II bands appear in the normal spectrum and carcinoma spectrum at 1640 cm^{-1}. The bands are more intense in the spectrum of normal samples in comparation with the carcinoma spectrum. Also, the contributions from lipids at 1454 cm^{-1} and from nucleic acids at 1239 cm^{-1} are more prominent in the spectrum characteristic to the cancerous samples.

In Fig. 3.2 the FT-IR spectra of the white part characteristic to the mucosa layer from normal and cancerous samples are presented. The amide I band present at 3287 cm^{-1} is more intense in the spectrum of normal tissues than the one corresponding to cancerous samples. The CH_2 antisymmetric stretching modes of mainly lipids is seen at 2926 cm^{-1} in the cancerous tissue while in the normal mucosa this mode appears shifted at 2923 cm^{-1}. This mode and the CH_2 symmetric stretching mode of lipids which remains constant in both samples at 2853 cm^{-1} are less intense in the normal tissue compared to the cancerous one.

In the fingerprint region, 1800–650 cm^{-1}, the differences in the two spectra lie in the relative intensity of the present bands, as well as new weak bands which appear in the spectrum of cancerous samples.

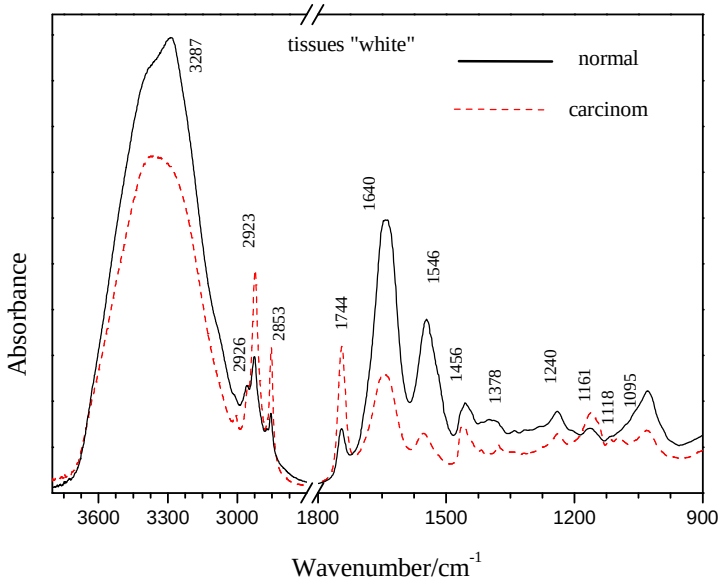

Fig. 3.2. ATR- FT-IR spectra of normal (upper) and carcinoma (lower) white tissues from human colon.

The C=O stretching mode of lipids at 1744 cm^{-1} in the spectrum of normal tissue is less intense and slightly shifted towards bigger wavenumbers, when compared to the one in the spectrum of carcinoma samples. The bands at 1640 cm^{-1} and 1546 cm^{-1} corresponding to amide I, C=O stretching mode and amide II, N–H bending and C–N stretching in proteins [71] have a higher intensity in the spectrum of normal tissues than in the one of cancerous ones.

Other contributions seen in the two spectra collected from the white zones of the samples are nucleic acids (1161 cm^{-1}), phospholipids (1240 cm^{-1}). Also, in the cancerous spectrum a new weak band appears at 1118 cm^{-1}. On the other hand, the vibrational modes 1378 and 1095 cm^{-1}, respectively appear more intense in the normal tissue.

The FT-IR spectra collected from the brown areas corresponding to the muscularis layer of the normal and cancerous samples are presented in Fig.3.3. In the big wavenumber region, the amide band seen at 3305 cm^{-1} is more intense in the spectrum of the normal samples. The asymmetric and symmetric contributions from lipids present at 2923 and 2854 cm^{-1}, respectively have smaller intensity in the normal than in the cancerous samples. In the fingerprint region the C=O stretching mode of lipids seen at 1744 cm^{-1} is less intense in the normal spectrum, while the contributions from amide I and II observed at 1640 and 1551 cm^{-1} are more intense when compared to the spectrum of the carcinoma samples, reminding of the same situation seen in the spectra collected from the white areas.

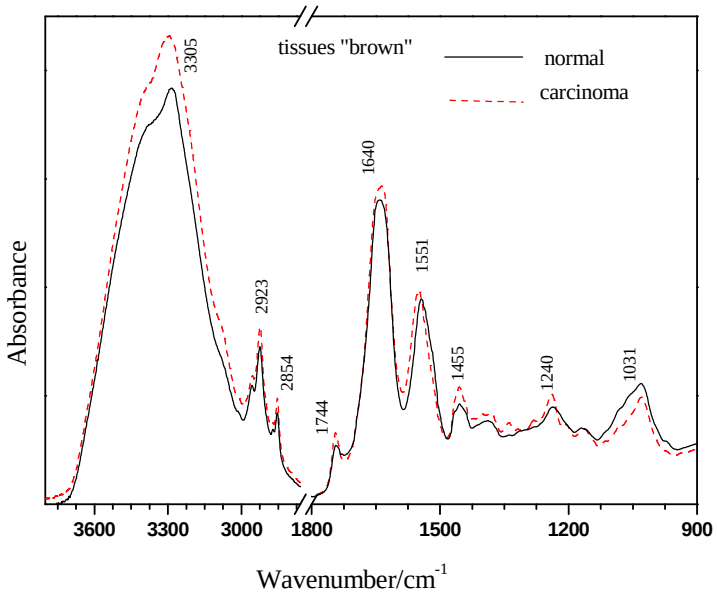

Fig. 3.3. ATR- FT-IR spectra of normal (lower) and cancerous (upper) tissues of human colon collected from the brown areas.

The characteristic bands of amide I and II of proteins were found to be of higher intensity in the spectra collected from the normal tissues, while the bands assigned to lipid contributions were more intense in the spectra acquired from cancerous areas.

3. 4. SERS measurements on healthy tissue and human colon cancer

In the last decade, Raman spectroscopy has been extensively used in biomedicine as a tool for diagnosis of tissue lesions, analysis of blood components, and study of single cells and tissues [72, 73]. In order to find a remedy to treat cancer, I applied surface enhanced Raman scattering (SERS) in order to evaluate the possibility of the technique to detect trace amounts of the rare-earth-acenocoumarol complexes and to investigate the adsorption behaviour of the complex to the Ag colloidal nanoparticles [74], because coumarins comprise a group of natural compounds of high interest for their anti-inflammatory, antioxidant, antiallergic, hepatoprotective, antithrombotic, antiviral, and anticarcinogenic activities

Characteristic SERS feature of epithelial layer from normal colon are displayed in Fig. 3.4, where the tissue fluorescence quenching upon visible laser excitation, due to the Ag nanoparticles is highlighted. A representative one collected in 20 s from a freshly sectioned sample upon adding 1 μl Ag colloid is presented in Fig. 3.4c, where as the micro-Raman spectra from the same collecting points before adding the Ag nanoparticles (Fig. 3.4d) exhibited only large fluorescence background, any Raman signal being completely covered.

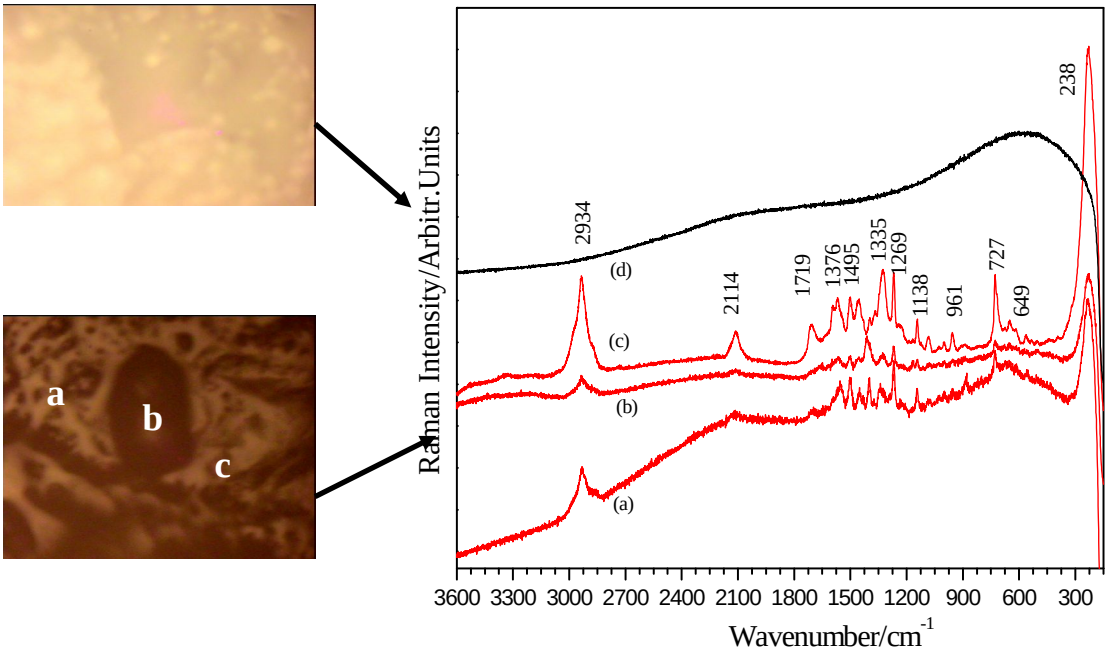

Fig. 3.4. Typical SERS spectra collected from normal colon epithelial layer (a–c), in comparison with the micro-Raman signal (fluorescence) from the same point as (c) before adding the Ag colloidal nanoparticles. Excitation: 632.8 nm, 25 mW (SERS), and 200 mW (Raman). The white light microscope images, before (top) and after (bottom) adding colloidal nanoparticles, indicate the locations at which the SERS spectra were acquired.

An impressive decrease in intensity of fluorescence background and clearly resolved sharp bands were observed on passing from Raman to SERS spectra. Typical SERS spectra from different random points of freshly sectioned carcinoma tissue are showed in Fig. 3.5. In spite of particular differences that reflect the inhomogeneity of the tissue, major bands at 1138, 1269, 1452, 1495, 1572, and 2934 $cm^{-1}$are representative for all the spectra. According to the SERS selection rules [75], vibrational modes with polarizability components perpendicular to the Ag surface are preferentially enhanced. Such modes clearly belong to the molecular species located in close vicinity or attached to the Ag nanoparticles. The major observed bands in the SERS spectra are tentatively assigned based on the previous Raman reports on normal colon and carcinoma tissue and on the recently reported Raman database of biological molecules [76]. In the carcinoma SERS feature, the most intense SERS band at 238 cm^{-1} is representative of the Ag-N mode when N-containing molecules are adsorbed on the Ag nanoparticles. Bands that are almost exclusively due to the ring breathing modes of the DNA and RNA bases, adenine (727, 1138, 1335, 1376, 1495 cm^{-1}), guanine (672 cm^{-1}), cytosine (1269 cm^{-1}), thymine (436, 617, 1495 cm^{-1}), and amino acids with cyclic R side chain (histidine–1575 cm^{-1}), phenylalanine (1002 cm^{-1})-this last band being specific also for tryptophan–are significantly enhanced.

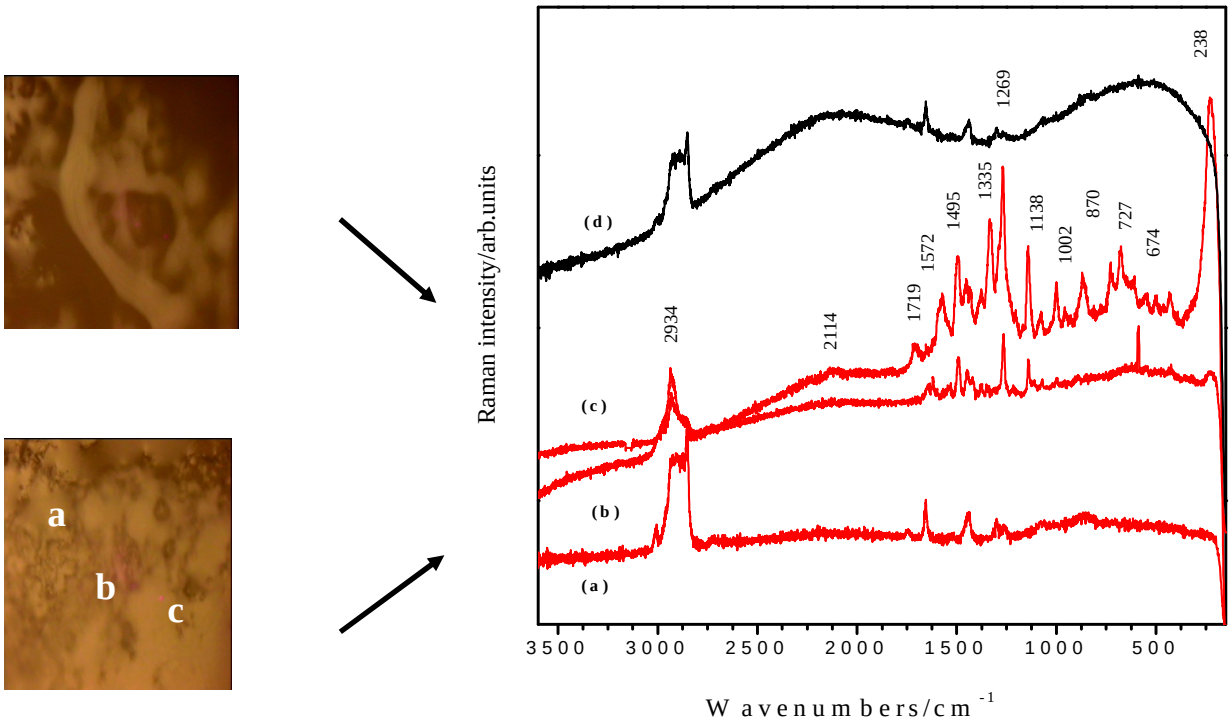

Fig. 3.5. Typical SERS spectra collected from colon adenomacarcinom tissue (a–c), in comparison with the micro-Raman signal (fluorescence) from the same point as (c) before adding the Ag colloidal nanoparticles. Excitation: 632.8 nm, 25 mW (SERS), and 200 mW (Raman). The white light microscope images, before (top) and after (bottom) adding colloidal nanoparticles, indicate the locations at which the SERS spectra were acquired.

The PO2_ stretching mode of the DNA backbone at 1069 cm^{-1} showed weak intensity. The absence of the amide I band from proteins in the 1600–1700 cm^{-1} spectral range is noteworthy. In the SERS spectrum of normal epithelial tissue (Fig. 3.4.c), sharp bands have been observed at 238, 727, 961, 1457, 1501, 1566, 1600, 1719, 2144, and 2934 cm^{-1}. Their band shape and relative intensity clearly differentiates the SERS behavior of normal and carcinoma tissue. In spite of the fact that most of them are attributable to nucleic acids, signal from proteins or lipids is also present. Comparing the different assignments of the previously reported Raman spectra of colon tissue, the data are still controversial. This fact is almost entirely due to the weak and complicated micro-Raman signal that resulted from direct measurement in FT or confocal configuration.

The unique ability of SERS technique to enhance the signal from molecular species located in the close vicinity of the Ag particles is now demonstrated for tissue measurements. Summarizing these findings, one can tentatively conclude that the nucleic acids are preponderantly present in the carcinoma tissue, proteins or lipids being less representative. However, such presumption would be further supported by the SERS tissue imaging, since the present results proved the possibility to record highly resolved bands from carcinoma tissue.

Therefore, information about DNA conformation and changes within the carcinogenic process, together with the decrease of protein content could be selectively extracted using SERS technique, without any dye labeling or other chemical species as functionalized binding sites [77]. Another major advantage of SERS-based investigation of tissue is the short acquisition time of the SERS spectra with much better signal-to-noise ratio, and a lower incident laser power than in the case of micro-Raman measurements. These preliminary results are of high interest in the nanoparticles-based SERS sensors for *in vivo* gastrointestinal early diagnostic and therapy monitoring.

Chapter 4. Raman spectroscopy of tissue samples prepared for histopathological examination

4. 1. Raman spectroscopic investigations of tissue taken from 9 patients diagnosed with diverese histopathological stages of cancer

In this study I expanded the Raman investigation to the stained soft tissue, using human tissue samples from 9 patients, aiming to probe the ability of the technique for simultaneous Raman and immunoshistochemistry diagnostic; to evaluate the influence of the staining agents on the tissue Raman signal; and to probe the specificity from one patient to another. Therefor, we recorded and discuss here the Raman signal from H&E stained and formaline fixed tissue respectively, from both normal tissue and cancer in different stages, as revealed by the histopathology. The H&E, xylene and *Biomont* resin involved in the staining protocol have been also Raman analyzed, to assist the correct interpretation of the results. I selected normal human colon and carcinoma tissue samples in this study, taking into account its increasing incidence in population and drastic demand for sensitive techniques to assist excision of lesions and residual tissue, predict the demarcation limit between healthy and tumor tissue and to understand the molecular changes associated to carcinogenesis. Completeness of excision as judged by the endoscopist on histopathologist could be sensitively assisted by the appropriate Raman spectroscopy technique in real time Raman spectroscopy, as a fast and reliable technique for rapid and sensitive diagnostic has recently showed promised results in the field [78-82].

However, the current routine analysis is based on the golden standard. According to the above cited document [83], there are currently no validated methods of determining completeness of excision

In this sense, Raman Spectroscopy technique would be able to perform quantitative and qualitative analysis since it shows high sensitivity to subtle structural changes in biological tissues.

Standard histopathological examination confirmed adenocarcinoma from 9 patients undergoing surgical intervention. As a routine procedure, upon surgical intervention, tissue segments considered - normal are usually removed, due to the lack of sensitive technique that could assist the intervention and clearly delimitate the normal from pathological tissue. As such, the histopathology normal tissue collected from the 9 patients has been also investigated. The mean FT-Raman spectra collected from the epithelial layer of the formalin fixed colon tissue have been recorded from each of the 9 cases, as shown in the Fig .4.1a, with spectral offset for clarity, whereas those corresponding to the cancer tissue are shown in the Fig. 4.1b (no spectral offset, to evidence the patient specificity).

The spectra were collected from normal regions which have been excised along with the cancerous ones. Each FT-Raman spectrum was an average value of 500 scans fromrandom points of the tissue slides. I can note that both normal and cancer samples exhibit two main different spectral shapes, as shown in the Fig. 4.2. The systematic differences in the high wavenumber range between randomly investigated points of each tissue sample are explained based on the previous results on cells [84].

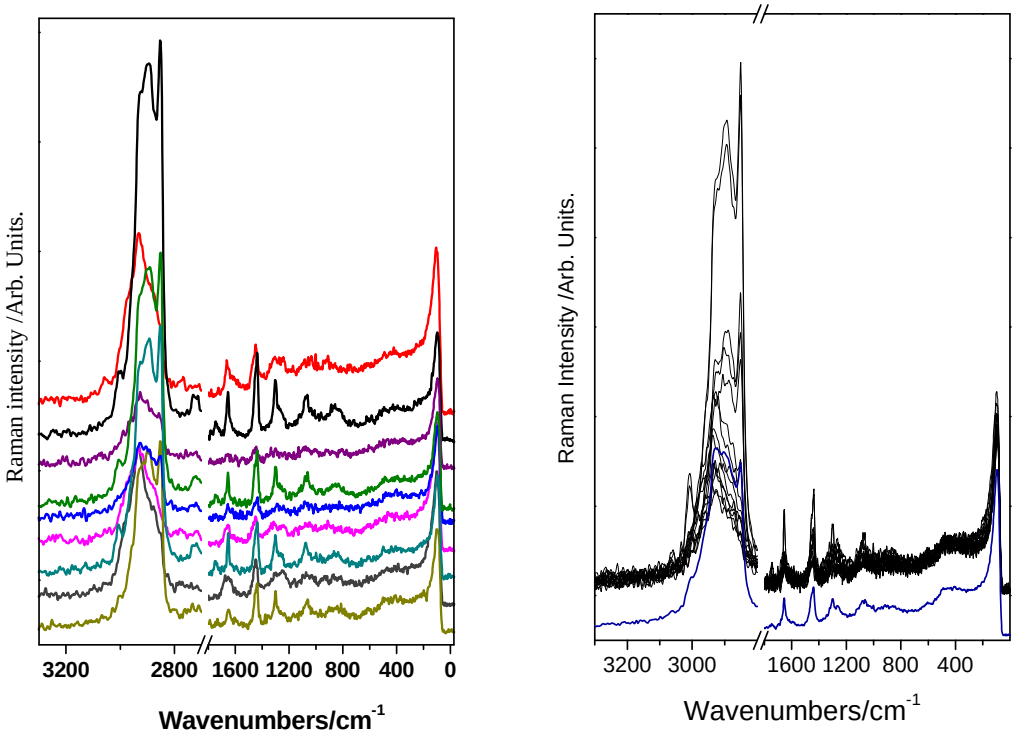

a) b)

Fig. 4.1. a) Mean signal of the FT-Raman spectra collected from each normal colon tissue sample from 9 patients, after formalin fixation. Spectral offset was introduced for clarity. b) Mean FT-Raman signal collected from the formalin fixed cancer tissue from 9 different patients. The insertion highlights the spectral differences in the fingerprint region.
Excitation: 1064 nm, 350 mW.

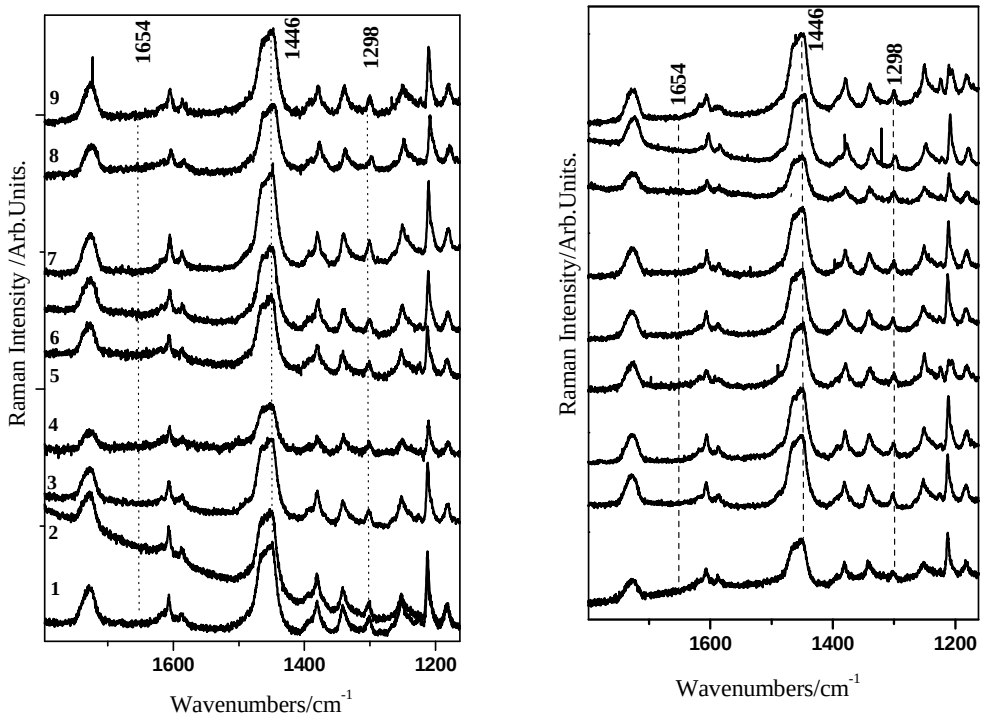

Fig. 4. 2. Micro-Raman spectra collected from H&E stained normal (top) and cancer (bottom) tissue from the 9 patients. Excitation: 632 nm, 3 mW. The spectra are displayed from 1 to 9 according to the increasing degree of metastases from cancer stage B (spectra 1-5), stage C (spectra 6-8) and stage D (spectrum 9).

The observed bands in the 600-1800 cm^{-1} range in Fig. 4.1a are discussed in comparison with the previous FT-Raman report on normal colon tissue [85]. Due to the inherent inhomogeneity of the tissue, from one point to another, the signal presents slice differences, however, the statistical analysis revealed specific spectral fingerprint for specific sample goups.

As shown by Andrade et al [85], the tissue content present great variations for different people, which reflect the intrinsic biological variability of the individuals, however, the main bands are still observed in all spectra. As an overall conclusion, the raw FT-Raman signal exhibits constant characteristic bands from one sample to another.

Raman spectra of the stained tissue in the 1800-1100 cm^{-1} range are presented in the Fig. 4.3, for both normal (a) and carcinoma (b) groups. The overall Raman signal of the H&E stained tissue is a superposition of the fluorescence background and Raman scattering of tissue, as well as the Raman (pre-resonance Raman) of the staining agents, as shown in the raw, unprocessed signal of one sample in Fig. 4.4. The corresponding FT-Raman signal of the same sample is also given for eye guidance (Fig. 4.4, bottom) and the main bands were followed in the signal from stained tissue. We noted many additional bands, revealing the

Raman contribution of the staining agents. These contributions were analyzed by recording and comparing the FT-Raman signal from hematoxylin, eosin, xylene and *Biomont*, as they used in the clinical laboratories.

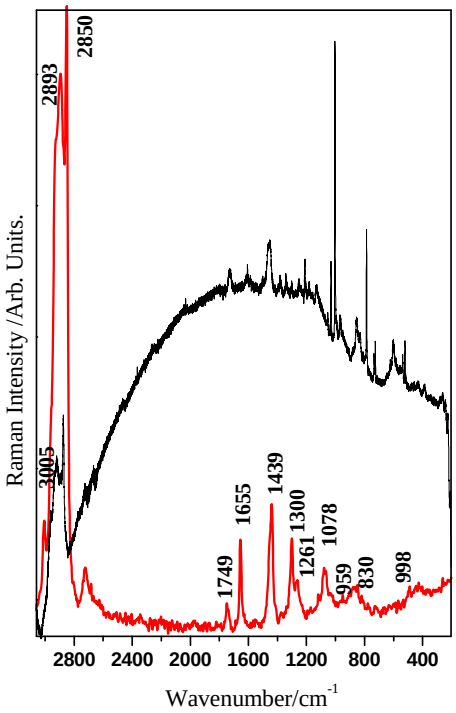

Fig. 4.3. Typical raw, unprocessed Raman signal recorded from H&E stained normal colon tissue (top) revealing additional bands compared to those of the unstained one, formalin fixed tissue.
Excitation: 632.8 and 1064 nm.

The *Biomont* exhibit Raman bands at 3047, 2915, 2876, 2731, 1732, 1611, 1450, 1378, 1249, 1202, 1092, 1029, 996, 832, 640, 533 cm^{-1}. The sharp interferences are also observed from xylene at 1611, 1378, 1092, 1029, 996, 1202, 823, 721, 640, 533, 456 cm^{-1} as well as in the 2876-3047 cm^{-1} range.

In order to evaluate the interference effects of the staining agents in the Raman spectra of tissue, the Raman signal of the formalin fixed tissue has been compared to that of the H&E stained sample from the same patient as well as with the individual staining agents (Fig. 4.4). The most representative FT-Raman bands of the formaline fixed tissue are shown with dotted lines, for guidance. Surprisingly, the main H&E bands were not observed in the stained tissue signal (Fig. 4.4).

Moreover, we noted the absence of the amide I band at 1654 cm-1 in the spectra of the stained tissue as well as the prominent appearance of the band at 1723-1749 cm^{-1}. This aspect could be probably correlated with the cell necrosis, where the proteins are destroyed. However, the absence of amide I band was observed either for normal tissue. On the other hand, during the tissue processing the proteins are denaturated by coagulation and polymerization reactions, resulting in blockage and stop the enzymatic reactions and autolyse. The prominent tissue band at 1446 cm^{-1} (Fig. 4.4) seems to be unaffected by the staining agents signal. Therefor, their intensity monitoring would be suitable for further Raman

imaging studies that could complementary assist the correct histopathology conclusions. It should be pointed out that this band was proposed as a marker of malignancy in Raman diagnostic of colorectal adenocarcinoma cell lines [84].

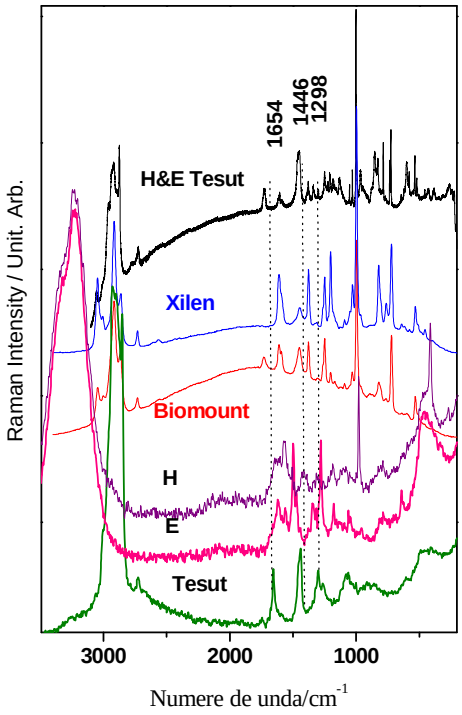

Fig. 4.4. Raman signal of the species involved in the staining protocol (H-hematoxylin, Eeosin, xylene and *Biomount*), as shown on each spectrum. The signal both from stained or formalin fixed tissue is also given for highlighting the spectral interferences. Spectral offset is introduced for clarity. The dotted lines followed the main bands of the unstained tissue. Excitation: 632 nm, 3 mW.

The high wavenumber range (3050-2800 cm^{-1} of the stained tissue spectra (Fig. 4.6) was found to be completely hampered by the xylene and *Biomont* contributions respectively, being impossible to use for diagnostic purpose. Usually, the CH_3 and CH_2 stretching modes of lipids at 2923 cm^{-1} and 2875 cm^{-1} respectively in the spectrum of cancer tissue are higher than in the case of normal tissue [85], indicating the increasing content of lipids as a characteristic self-defense reaction of the organism. This characteristic was also observed in the unstained tissue [84, 85, 86]. A previous report [87] showed the comparison of the Raman spectra of fresh tissue with formalin fixed tissue and tissue fixed and soaked in xylene. A dramatic reduction in the intensity of the amide I band (1637 cm^{-1}) was observed for the formalin tissue whereas soaking in xylene prior to wax embedding creates significant spectral differences in the tissue.

Although every tissue processing step introduced significant changes in the Raman signal, the authors concluded that the dewaxed sections can be diagnostically useful, since they retain sufficient biochemical similarity to the fresh one, drawing the conclusion of awaring when used automated processing techniques. H&E stained tissue provide all the dewaxed tissue information. Another report was devoted to improve the de-waxing protocol [88]. Cervical tissue samples were prepared in multiple dewaxing cycles, using xylene, Histoclear and hexane.

However, the present Raman results on H&E stained tissue proving the possibility to record specific tissue signal, open new perspective for Raman diagnostic techniques, with higher spatial resolution, in order to be able to differentiate the nuclear and cellular components which are optically revealed by the H&E staining.

Conclusions

• With vibrational spectroscopy and we could differentiate the two forms of paracetamol, respectively monoclinic form (commercial) and orthorhombic form.

• It was highlighted the fact that after recrystallization normal paracetamol can contain a mixture of two forms, while the sinus paracetamol only contains the monoclinic form.

• The most important bands of certain ingredients, added in the preparation of medicines, could be identified.

• It was deducted the interaction of paracetamol molecule with the Ag film surface through several functional groups.

• Using vibrational spectroscopy, it was proven that we can identify key molecular components in the samples studied and their molecular modification, thus allowing the differentiation between normal and cancerous tissue of the human colon.

• It was shown that normal tissues have higher protein content, while the cancerous tissues were characterized as having lower protein content and higher lipid content.

• By analyzing the spectra obtained in the three areas under study, respectively mucosa, sub mucosa and muscle it could be evidenced that, cancer extends from inside to outside.

• In principle, if we rely on assumptions provided by the data provided, it is possible to conclude that FT-IR-Raman spectroscopy shows great promise in terms of methods of diagnosing cancer and could be used as a classification system of the tissue.

• After obtaining a SERS signal it can be said that combining the micro-Raman technique with the plasmonic properties of appropriate noble metal nanoparticles, we can achieve real progress towards a new platform based on endoscopy SERS, which is to study the complex biochemical mechanisms of carcinogenesis and therefore high effective early diagnosis of disease.

• Analyzing micro-Raman spectra of tissue stained with H & E (case study 9 patients), could shown that H & E does not have strips to interfere drastically the strips obtained from the tissues.

• Bands from Xilenn and resins interfere with tissue bands, but even so, a few bands remain unaltered, specific to pure biological tissue, non treated with preservatives and unmarked, and can be used in Raman investigations.

References :

1. J. R. Mitchell, D. J. Jollow, W. Z. Potter, D. C. Davis, J. R. Gilette, B. B. Brodie, *J. Pharm. Exp. Ther.*, 1973; **187**: 185.
2. S. Morgan, S. Dorman, *Letters,* 2004; **27**: 99-101.
3. C. H. Lorén, P. Thesleff, A. Nilsson, *Med. Scand.*, 1987; **222**: 185-288.
4. J. A. Hinson, In *Reviews in Biochemical Toxicology E.* Hodgson, J. R. Bend, R . M. Philpot Eds., Elsevier, Amsterdam, 1980; **2**: 103-129.
5. M.W. Gemborys, G. W. Gribble, G. H. Mudge, *J. Med. Chem.*, 1978; **21**: 649-656.
6. C. H. Florén, P. Thesleff, A. Nilsson, *Med. Scand.* 1987; **222**: 185-288.
7. J. A. Hinson, In *Reviews in Biochemical Toxicology,* E. Hodgson, J. R. Bend , R. M. Philpot Eds., Elsevier, Amsterdam, 1980; **2**: 103-129.
8. M. W. Gemborys, G.W. Gribble, G. H. Mudge, *J. Med. Chem.* 1978; **21**: 649-652.
9. D. P. Sandler, J .C. Smith, C. R. Weinberg, Y. M. Buckalew, V. W. Dennis, W. B. Blythe, W. P. Burgess, *N. Engl. J. Med.* 1989; **320**: 1238.
10. A. M. Richard, J. K. Hongslo, P. F. Boone, J. A. Holme, *Chem. Res. Toxicol.* 1991; **4**: 151-156.
11. P. Di Martino, P. Conflant, M. Drache, J. P. Huvenne, A. M. Guyot-Hermann, *J. Therm. Anal.* 1997; **48**: 447-458.
12. T. Beyer, G. M. Day, S. L. Price, *J. Am. Chem. Soc.* 2001; **123**: 5086-5094.
13. A. Rossi, A. Savioli, M. Bini, D. Capsoni,V. Massarotti, R. Bettini, A. Gazzaniga , M. E. Sangalli, F. Giordano, *Therm. Acta* 2003; **406**: 55-67.
14. M. L. Peterson, S. L. Morissette, C. McNulty, A. Goldsweig, P. Shaw, M. LeQuesne, J. Monagle, N. Encina, J. Marchionna, A. Johnson, J. Gonzalez-Zugasti, A. V. Lemmo, S. J. Ellis, M. J. Clima, J. Almarsson, *J. Am. Chem. Soc.* 2002; **124**: 10958-10959.
15. M. Szelagiewicz, C. Marcolli, S. Cianferani, A. P. Hard, A. Vit, A. Burkhard, M. Von Raumer, U. C. Hofmeier, A. Zilian, E. Francotte, R. Schenker, *J. Therm. Anal. Cal.* 1999; **57**: 23-43.
16. L. Kalantzi, C. Reppas, J. B. Dressman, G. L. Amidon, H. E. Junginger, K. K. Midha, V. P. Shah, S.A. Stavchansky, D. M. Barends, *J. Pharm. Sci.* 2006; **95**: 4-14.
17. F. P. A. Fabbiani, D. R. Allan, W .I. F.David, S. S. Moggach, S. Parsons, C. R. Pulham, *Cryst. Eng. Comm.* 2004; **6**: 504.
18. G. Nichols, C. S. Frampton, *J. Pharm. Sci.* 1998; **87**: 684-693.
19. P. Verwer, F. J. J. Leusen, *Revs. Comp. Chem.* 1998; **12**: 327-365.
20. P. Espeau, R. Céolin, J. L. Tamarit, M. A. Perrin, J. P. Gauchi, F. Leveiller, *J. Pharm. Sci.* 2005; **94**: 524-539.
21. A. J. Florence, N. Shankland, K. Shankland, W. I. F. David, E. Pidcock, X. Xu, A. Johnston, A. R. Kennedy, P. J. Cox, J. S. O. Evans, G. Steele, S. D. Cosgrove, C .S. Frampton, *J. Appl. Cryst.* 2005; **38**: 249-259.
22. F. Giordano, A. Rossi, R. Bettini, A. Savioli, A. Gazzaniga, C. Novák, *J. Therm. Anal. Cal.* 2002; **68**: 575-590.
23. H. A. Garekani, J. L. Ford, M. H. Rubinstein, A. R. Rajabi-Siahboomi, *Int. J. Pharm.* 2000; **208**: 87-99.
24. K. V. R.Prasad, R. I. Ristic, D. B. Sheen, J. N. Sherwood, *Int. J. Pharm.* 2002; **238**: 29-41.
25. M. A. Mikhailenko, *J. Cryst. Growth* 2004; **265**: 616-618.
26. P. A. McGregor, D. R. Allan, S. Parson, C. R. Pulham, *J. Pharm. Sci.* 2002; **91**: 1308-1311.

27. I. G. Bine, P. Vassileva-Boyadjieva, Y. I. Binev, *J. Mol. Struct.* 1998; **447**: 235-246.
28. M. L. Ramos, J.F.Tyson, D. L. Curran, *Anal. Chim. Acta* 1998; **364**: 107-116.
29. P. Merckle, K. A. Kovar, *J. Pharm. Biomed. Anal.* 1998; **17**: 365-374.
30. A. Eustaquio, M. Blanco, R. D. Jee, A. C. Moffat, *Anal. Chim. Acta* 1999; **383**: 283-290.
31. S. Y. Lin, S. L. Wang,Y. D. Cheng, *J. Phys. Chem. Solids* 2001; **61**: 1889-1893.
32. H. A. Moynihan, I. P. O'Hare, *Int. J. Pharm.* 2002; **247**: 179-185.
33. R. Szostak, S. Mazurek, *Analyst* 2002; **127**: 144-148.
34. **L. M. Andronie**, S. Canta, O. Cozar, I. Domsa Proceeding of the Physics Conference, Timisoara 28-29 (M. Bunoiu, I. Malaescu Eds.) p.191-196 (ISBN 978-0-7354-0668-1, ISSN 0094-234X) American Institute of Physics, Melville, New–York, 2009.
35. N. Peica, S. Cîntă Pînzaru, T. Frosch, M. Schmitt, J. Popp, G. Bringmann, W. Kiefer, Proceedings "3rd International Conference on Materials for Advanced Technologies" (ICMAT), International Union of Materials Research Societies, "9rd International Conference on Advanced Materials" (IUMRS–ICAM), *Singapore*, Singapore, Book of abstracts, (2005) July, 3-8.
36. M. L. Peterson, S. L. Morissette, C. McNulty, A. Goldsweig, P. Shaw, M. LeQuesne, J. Monagle, N. Encina, J. Marchionna, A. Johnson, J. Gonzalez-Zugasti, A. V. Lemmo, S. J. Ellis, M. J. Clima, J. Ö. Almarsson, *J. Am. Chem. Soc.*, 2002; **124**: 10958-10959.
37. M. Szelagiewicz, C. Marcolli, S. Cianferani, A. P. Hard, A. Vit, A. Burkhard, M. Von Raumer, U. C. Hofmeier, A. Zilian, E. Francotte, R. Schenker, *J. Therm. Anal. Cal.*, 1990; **57:** 23-43.
38. G. G. Mohamed, N. E. A. El-Gamel, F. Teixidor, *Polyhedron*, 2001; **20:** 2689-2696.
39. S. L. Wang, S. Y. Lin, Y. S. Wei, *Chem. Pharm. Bull.*, 2002; **50**: 153-156.
40. S. Romero, P. Bustamante, B. Escalera, M. Cirri, P. Mura, *J. Therm. Anal. Cal.*, 2004; **77**: 541-554.
41. B. B. Ivanova, *J. Mol. Struct.*, 2002; **738**: 233-238.
42. H. A. Moynihan, I. P. O'Hare, *Int. J. Pharm.*, 2002; **247**: 179-185.
43. M. F. Mrozek , S. A. Wasileski, M. J. Weaver, *J. Am. Chem. Soc.* 2001; **123**: 12817.
44. F .C. Thorley, K. J. Baldwin, D. C. Lee, D. N. Batchelder, *J. Raman Spectrosc.* 2006; **37**: 335-341.
45. J. S. Day, H .G. M. Edwards, S. A. Dobrowski, A. M. Voice, *Spectrochim. Acta A* 2004; **60**: 563-568.
46. A. P.Terzyk, G. Rychlicki, S. Biniak, J .P. Łukaszewicz, *J. Colloid Interface Sci.* 2003; **257**: 13-30.
47. A. P. Terzyk *Colloids and Surfaces A,* 2001; **177**: 23-45.
48. A. Szép, P. Fekete, J. Virgula, Z. Budavári, G. Marosi, *Proceeding of the 8th Polymers for Advanced Technologies International Symposium*, Budapest, Hungary, 13-16 September 2005.
49. F. Clarke, A. Whitley, S. Mamedov, F. Adar, N. Lewis, E. Lee, *Spectroscopy-Solutions for Materials Analysis*, June 2005 AN ADVANSTAR PUBLICATION, Printed in U.S.A.
50. B. M. Murphy, S. W. Prescott, I. Larson, *J. Pharm. Biomed. Anal.*, 2005; **38**: 186-190.
51. H. Vogel, J. K. Wright, F. Jähnig, *The EMBO Journal*, 1985; **4:** 3625-3631.
52. P. M. Fechner, S. Wartewig, M. Füting, A. Heilmann, R. H. H. Neubert, P. Kleinebudde, *AAPS Pharm. Sci.*, 2003; **5**: 1-13.

53. S. J. Eichhorn, R. J. Young, *Cellulose*, 2001; **8:** 197-207.
54. U. P. Agarwal, *Appita*, 2005: 377-384.
55. R. H. Bisby, S. A. Johnson, S. M. Tavender, A. W. Parker, *Science-Lasers for Science Facility Programme*, CLF Annual Report 1996/1997.
56. B. M. Murphy, S. W. Prescott, I. Larson, *J. Pharm. Biomed. Anal.* 2005; **38**: 186-190.
57. H. Vogel, J. K. Wright, F. Jinig , *The EMBO Journal* 1985; **4**: 3625-3631.
58. P. M .Fechner, S. Wartewig, A. Heilmann,R. H .H. Neubert, P. Kleinebudde, *AAPS .Pharm. Sci.* 2003; **5**: 1.
59. S. J. Eichhorn, R. J. Young, *Cellulose* 2001; **8**: 197-207.
60. U.P. Agarwal, *Appita* 2005; **2005**: 377-384.
61. A. Wang A, Freeman J, Kuebler KE. *Lunar and Planetary Science* 2002; XXXIII: 1374.
62. A. P. Terzyk, *J. Colloid Interface Sci.* 2004; **272**: 59-75.
63. J. E. M. Diniz, R. S. Borges,C. N. Alves, *Theochem* 2004; **673**: 93-97.
64. **L. M. Andronie**, S. Canta, N.Peica, N. Leopold, O. Cozar, *Studia Universitatis Babes-Bolyai, Physica* 2, LIV, 2009, p.51-59.
65. J. A. Creighton, *Spectroscopy of Surface*, R. J. H. Clark, R. E. Hester (Eds.), Wiley, New York, 1988, pp. 37.
66. M. Moskovits; J. S. Suh, *J. Am. Chem. Soc.*, 1986; **108:** 4711.
67. S. Canta, **L. M. Andronie,** M**.** Baia, O. Cozar, Proc. 4-th International Conference: on Advanced Vibrational Spectroscopy (ICAVS), Corfu, Greece, 2007: 278.
68. P. C. Lee, D. Meisel, *J. Phys. Chem.* 1982; **86**: 3391.
69. M. Diem, S. Boydston-White, L. Chiriboga, *Appl. Spectrosc*., 1999; **53**: 148–161.
70. X.-Y. Wang, J. M. Garibaldi, B. Bird, M. W. George, *Applied Intelligence*, 2007; **27**: 237–248.
71. S.B. Akkas, M. Severcan, O. Yilmaz, F. Severcan, Effects *Food Chemistry*, 2007; **105**: 1281–1288.
72. .S. Caınta Paınzaru, **L. M. Andronie**, N. Peica, O Cozar, W. Kiefer. *Proceedings of the XX International Conference on Raman Spectroscopy (ICORS)*. Yokohama, Japan, 2006; 383.Chan JW, Taylor DS, Zwerdling T., Lane SM, Ihara K, Huser T. *Biophys.J*, 2006; 648.
73. L. P. Choo-Smith, H. G. M. Edwards, F. Heule, H. Barr, Biopolym (Biospectrosc) 2002; 648.
74. **L. M. Andronie**, S. C. Pînzaru, I. Kostova, O .Cozar, *Proc. of the XXII International Conference on Raman Spectroscopy (ICORS) Boston, USA*, 2010, 1045-1046.
75. De Gelder J, De Gussem K, Vandenabeele P, Moens L. *J. Raman Spectrosc.* 2007; **38**: 1133.
76. J. A. Creighton, *Spectroscopy of Surfaces*., Chapter. 2, R. J. H. Clark, R. E. Hester (eds). John Wiley & Sons: Chichester, 1988; 37.
77. S. Cîntă, **L. M. Andronie**, I. Domsa, O. Cozar, S. Astilean, *Journal of Raman Spectroscop*y, 2008; **39**: 331-334.
78. K. Chen, Y. Qin, F. Zheng, M. Sun, D. Shi, *Opt. Lett*. 2006; **31**: 2015-2017.
79. A. Molckovsky, L.-M. Wong, K. Song, M. G. Shim, N. E. Marcon, B. C. Wilson, *Gastrointestinal Endoscopy*, 2003;V57 (3): 396-402.
80. E. Widjaja, W. Zheng, Z. Huang, *Int. J. Oncol*. 2008**; 32**: 653-662.
81. T. C. Bakker Schut, M. J. Witjes, H. J. Sterenborg, O. C. Speelman, J. L. Roodenburg, E. T. Marple, H. A. Bruining, G. J. Puppels, *Anal Chem*, 2000; **72**: 6010-6018.

82. M. A. Short, H. Lui, D. McLean, H. Zeng, A. Alajlan, X .K. Chen, *J. Biomed. OpticS 2006;* 11(3): 34004-34013.
83. European Guidelines for Quality Assurance in Colorectal Cancer Screening and Diagnosis, First Edition., (Eds) N. Segnan J. Patnick L. von Karsa, Brussels, Publications Office of the European Union, 2010, 191-232. doi: 10.2772/15379, http://www.uegf.org/eu_affairs/eu_news/CRC_guidelines_publication%20EU_2011.pdf..
84. C. Scalfi-Happ, M. Udart, C. Hauser, A. Ruck, *Med. Laser Appl*. 2011; **26**: 152-157
85. P. O. Andrade, R .A. Bitar, K. Yassoyama, H. Martinho, A. M. E. Santo, P. M. Bruni, A. A. Martin, *Anal.Bioanal.Chem*.2007; **387**: 1647.
86. S. Pînzaru, **L. M. Andronie**, I. Domsa, O. Cozar, S. Astilean, *J. Raman Spectrosc*. 2008; **39**: 331–334.
87. A. Tuer, D. Tokarz, N. Prent, R. Cisek, J. Alami, D. J. Dumont, L. Bakueva, J. Rowlands, V. Barzda, *J. Biomed.Opt* 2010; **15**: 026018**.**
88. E. O Faola´in, M. B. Hunter, J. M. Byrne, P. Kelehan, M. McNamara, H. J. Byrne, F. M. Lyng, *Vib. Spec*. 2005; **38**: 121–127.

Mulţumiri,

Mulţumesc tuturor celor care m-au susţinut şi m-au încurajat în realizarea tezei de doctorat atât de importantă pentru mine şi viitorul meu.

Alese mulţumiri conducătorului ştiinţific al acestei teze de doctorat, domnul Prof. Univ. Dr. Onuc Cozar pentru sprijinul permanent pe care mi l-a acordat în toată această perioadă de studiu.

Mulţumiri speciale doamnei Conf. Dr. Simona Cântă-Pânzaru pentru contribuţia la formarea mea profesională, sprijinul moral, colaborarea fructuoasă, îndrumarea şi ajutorul acordat pe parcursul întregii perioade de cercetare şi elaborare a tezei de doctorat.

Mulţumesc întregului colectiv din cadrul Universităţii Babeş-Bolyai, acultatea de Fizică, departamentul *Spectroscopie Moleculară şi Teoretică*: Prof. Dr. Vasile Chiş, Prof. Dr. Leontin David, Prof. Dr. Simion Aştilean şi colegilor care mi-au oferit sprijinul şi prietenia lor.

Mulţumiri speciale Prof. dr. Wolfgang Kifer pentru colaborare şi facilitarea accesul la laboratoarele de cercetare din cadrul *Institut für Physikalische Chemie der Universität Würzburg, Germania*, şi celor cu care am colaborat pe parcursul acestor ani la editarea şi elaborarea publicaţiilor: Dr. Niculina Peica (Institut für Festkörperphysik, Technische Universität Berlin, Germany), Conf. Dr. Nicolae Leopold (Fac. de Fizica, Univ. Babeş-Bolyai, Cluj-Napoca, Romania), Dr. Ioan Domsa (Spitalul Universitar CFR, Dep. Anatomie Patologică, Cluj-Napoca, România), Prof. Dr. I. Kostova (Department of Chemistry, Faculty of Pharmacy, Medical University, Sofia, Bulgaria).

Nu în ultimul rând, datorez mulţumiri familiei mele, mamei şi tatălui meu, pentru atenţia, suportul, încurajarea şi dragostea oferită.

Dedic această lucrare fetelor mele dragi Ştefania şi Teodora, care au înţeles importanţa şi scopul acestei lucrări în viaţa mea, şi care îmi oferă dragostea lor necondiţionată.